Simulation of Poroelastic Wave Propagation Using CLAWPACK

Grady Lemoine, University of Washington

June 28, 2012

Joint work with Randall LeVeque (University of Washington) and M.-J. Yvonne Ou (University of Delaware)

Supported in part by grants from the NIH and NSF

Outline

Outline

Poroelasticity theory

- Poroelasticity: study of mechanics of fluid-filled porous solids
- Originally developed by Maurice Biot in 1930s-1960s for soil and rock
  - Major early interest from oil industry
  - Recent interest for monitoring underground fluid injection (e.g. carbon sequestration)
- Recently applied to bone as well
  - Understanding wave propagation in bone is original motivator for this work

Pumice stone.

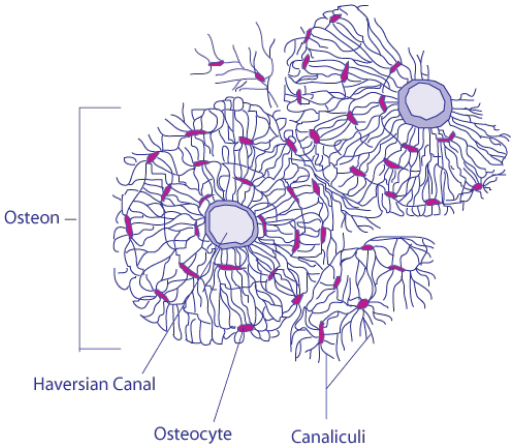

Transverse section of cortical bone. Images courtesy Wikimedia Commons.

Equations of poroelasticity

Glossing over a lot of details, can model poroelasticity as a first-order linear system of PDEs:

$$\partial_t Q + A\,\partial_x Q + B\,\partial_z Q = DQ,$$

$$Q = \begin{bmatrix} p & \sigma_{xx} & \sigma_{zz} & \sigma_{xz} & v_x & v_z & q_x & q_z \end{bmatrix}^T$$

- p is fluid pressure; σ is solid stress tensor; v is solid velocity; q is fluid flow rate
- These are in principal coordinates of orthotropic (*not* isotropic) material.
- Left side is classic hyperbolic system
- Right side introduces dissipation, through viscous drag as fluid flows through pores

▸ Show system matrices

Poroelastic waves

Poroelasticity equations look like elastodynamics + acoustics.
Three families of propagating waves:

1. **Fast P-waves**, where fluid and solid move (roughly) parallel to propagation direction and in phase
2. **S-waves**, where fluid and solid move transverse to propagation direction
3. **Slow P-waves**, where fluid and solid move (roughly) parallel to propation direction but 180 degrees out of phase

Slow P-waves involve large motions of fluid relative to solid – heavily damped by viscosity
System also supports non-wave-like “diffusive slow mode” where fluid seeps through pores due to pressure gradient

Wave structure of viscous orthotropic poroelasticity

Source term DQ causes dissipation and dispersion
Anisotropy also causes wave speeds to differ depending on propagation direction
Plots below: phase velocity vs. frequency and direction for orthotropic layered sandstone

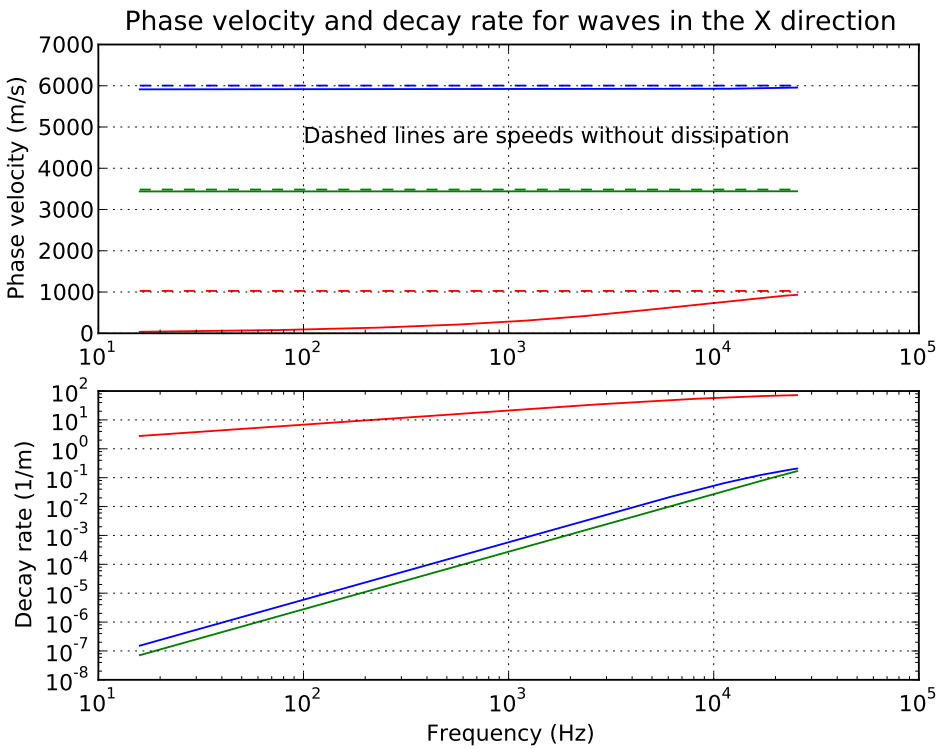

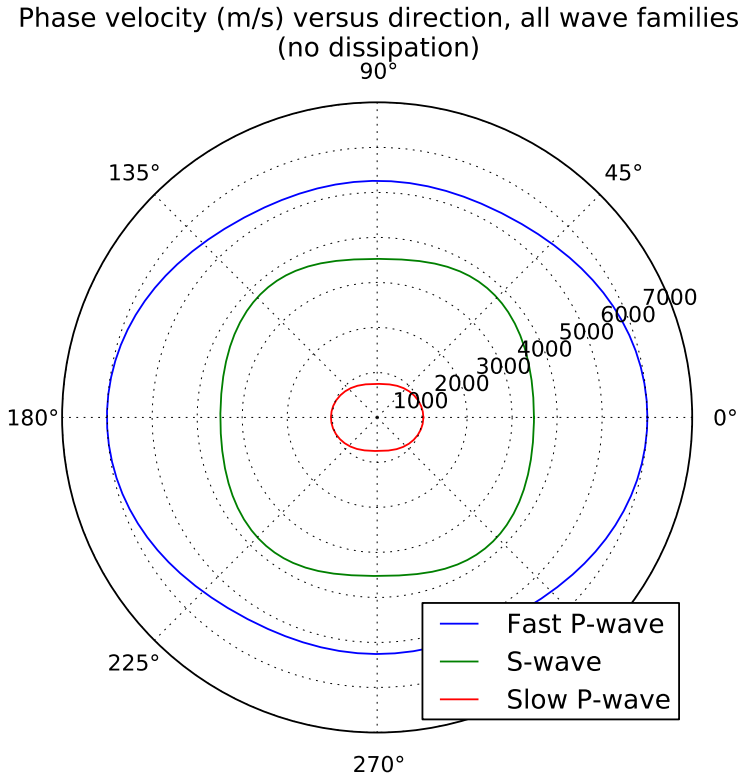

Energy density

- Poroelasticity system has some useful properties
- Several are associated with the energy density $\mathcal{E}$, which is a quadratic form,

$$\mathcal{E} = \frac{1}{2} Q^T E Q$$

- Hessian E is a symmetric positive-definite matrix
- E symmetrizes the system: EA, EB, and ED are symmetric
- Easy proof poroelasticity system is hyperbolic
  - Eigenvalues and eigenvectors of $\breve{A} = n_x A + n_z B$ satisfy symmetric-definite generalized eigenproblem $E\breve{A}v = \lambda E v$
  - $\Rightarrow$ Have all real eigenvalues, full set of independent (E-orthogonal) eigenvectors, therefore hyperbolic

▸ Show energy matrix

Block structure of poroelasticity system

Aside: poroelasticity system has stress-velocity block structure

- Have grouped stress and velocity variables in state vector to emphasize this:

$$Q = \begin{bmatrix} p & \sigma_{xx} & \sigma_{zz} & \sigma_{xz} & v_x & v_z & q_x & q_z \end{bmatrix}^T = \begin{bmatrix} Q_s \\ Q_v \end{bmatrix}$$

- A, B matrices — stress gradients produce velocity changes, velocity gradients produce stress changes:

$$A = \begin{bmatrix} 0 & A_{sv} \\ A_{vs} & 0 \end{bmatrix}, \quad B = \begin{bmatrix} 0 & B_{sv} \\ B_{vs} & 0 \end{bmatrix}$$

- Energy divides neatly into kinetic and potential:

$$E = \begin{bmatrix} E_s & 0 \\ 0 & E_v \end{bmatrix}$$

This will be useful later

Stiffness of relaxation term

$$\partial_t Q + A\,\partial_x Q + B\,\partial_z Q = DQ$$

- Source term DQ has its own intrinsic time scales
- May be stiff depending on problem solved
- Can expect difficulties with solution, need to check for possibility of incorrect wave speeds
- Source term is of relaxation type, so expect solution to be close to *reduced system*,

  $$\partial_t u + A_r\,\partial_x u + B_r\,\partial_z Q = 0$$

  obtained by restricting to null space $\mathcal{N}(D)$
  - $A_r = \Pi A G$, where G maps reduced variables to full variables and Π maps full to reduced
- Conjecture (Pember 1993): Need reduced system to satisfy *subcharacteristic condition* – wave speeds not faster than full system

Entropy function and subcharacteristic condition

$\mathcal{E} = \frac{1}{2} Q^T E Q$ turns out to be a *strictly convex entropy function* in the sense of Chen, Levermore, and Liu (1994).

1. EA and EB are symmetric
2. ED is symmetric negative-semidefinite
3. The following are equivalent:
   - $Q \in \mathcal{N}(D)$
   - $Q^T E D Q = 0$
   - $EQ = \Pi^T v$ for some v
4. E is positive-definite

Chen, Levermore, and Liu show this implies a nonstrict subcharacteristic condition,

$$\lambda_{\min}(A) \leq \lambda_{\min}(A_r), \quad \lambda_{\max}(A_r) \leq \lambda_{\max}(A)$$

- Can expect to avoid spurious solutions
- Accuracy may still be affected

Outline

CLAWPACK

Solved poroelasticity equations using CLAWPACK

- CLAWPACK: Conservation LAWs PACKage
  - Can really handle any hyperbolic system, not just conservation laws
- High-resolution finite volume package for wave propagation
- Low memory overhead, parallel (multicore, PETSc)
- Supports logically rectangular mapped grids
- Source terms handled by operator splitting
- Adaptive mesh refinement available too (Berger-Colella-Oliger approach, AMRCLAW)
- Handles code that is common across all high-resolution FVM solvers
  - User only needs to write routines for Riemann solve, source terms

Riemann solver

Writing an efficient Riemann solver for this system looks hard:

- 8×8 system with 3 wave families – lots of computation per solve
- For applications, want to handle material heterogeneity
- Also want to handle mapped grids, arbitrary interface direction
- Can't use geometric symmetry – anisotropic material!

However, can take advantage of block structure, energy matrix to simplify

Riemann solver

- Waves and speeds come from eigenproblem $\breve{A}r = \lambda r$, where $\breve{A} = n_x A + n_z B$
- E is nonsingular, so multiply by E to get $E\breve{A}r = \lambda Er$
- From block structure of E and $\breve{A}$, get

$$E_s \breve{A}_{sv} r_v = \lambda E_s r_s, \quad E_v \breve{A}_{vs} r_s = \lambda E_v r_v$$

- Since $E\breve{A}$ is symmetric, $E_v \breve{A}_{vs} = (E_s \breve{A}_{sv})^T$. Rewrite second equation as

$$\breve{A}_{sv}^T E_s r_s = \lambda E_v r_v$$

- Multiply first equation by $\breve{A}_{sv}^T$ from left:

$$\breve{A}_{sv}^T E_s \breve{A}_{sv} r_v = \lambda \breve{A}_{sv}^T E_s r_s = \lambda^2 E_v r_v$$

- Reduced 8×8 problem to 4×4 symmetric definite problem

Riemann solver

- Can reduce to symmetric ordinary eigenproblem by factorizing E_v to LL^T:

$$L^{-1}\breve{A}_{sv}^T E_s \breve{A}_{sv} L^{-T} w \equiv M_4 w = \lambda^2 w, \quad w = L^T r_v$$

- M_4 matrix is complicated but can break down in terms of n_x and n_z:

$$\begin{aligned} M_4 = & L^{-1}A_{sv}^T E_s A_{sv} L^{-T} n_x^2 \\ & + (L^{-1}A_{sv}^T E_s B_{sv} L^{-T} + L^{-1}B_{sv}^T E_s A_{sv} L^{-T}) n_x n_z \\ & + L^{-1}B_{sv}^T E_s B_{sv} L^{-T} n_z^2 \\ & \equiv M_{4xx} n_x^2 + M_{4xz} n_x n_z + M_{4zz} n_z^2 \end{aligned}$$

- Can precompute M_{4**} matrices, only form linear combination at each solve
- Also know null space of $\breve{A}_{sv}$, can reduce dimension with variable substitution
- In the end, get 3×3 symmetric eigenproblem

Riemann solver

Finally, need breakdown of ΔQ into waves for Riemann solve

- Want to be able to solve at interface between two materials
- In general, need to solve linear system for wave strengths
- If material is same on both sides, can use E-orthogonality of eigenvectors instead
- Make eigenvectors E-orthonormal. Want to solve

$$R\alpha = \Delta Q$$

- Multiply from left by $R^T E$ to get

$$R^T E R\alpha = \alpha = R^T E \Delta Q$$

Source term

- Source term handled via operator splitting
- $Q_t = DQ$ solved exactly with matrix exponential
  - Best accuracy available for this part of system
  - No stability restriction
- Strang splitting used for all cases presented here
  - Expect second-order accuracy, but will see what we actually get...

Outline

Overview of results

Two general classes of test problems run so far:

1. Qualitative sanity-check problems and “eyeball norm” comparisons to published solutions
   - Advantage: Useful when analytic solution not available, good for ruling out some types of bug
   - Disadvantage: Not very precise
2. Convergence studies comparing against known analytic solutions
   - Advantage: Can quantitatively measure accuracy, convergence rate
   - Disadvantage: Limited library of solutions to compare against (just used plane waves here)

Both types of test are useful

Poroelastic code validation: two-material test case

Test case: wave reflections from a material interface, from de la Puente et al. (2008)

- Excitation is a point source with a Ricker wavelet profile in time
- Forcing acts on σ_z and fluid pressure terms with equal magnitude and opposite sign
- Source is located in shale overlying a sandstone bed
- Material properties taken to be isotropic for this case; viscosity ignored
- AMR used to capture fine details

Poroelastic code validation: two-material test case

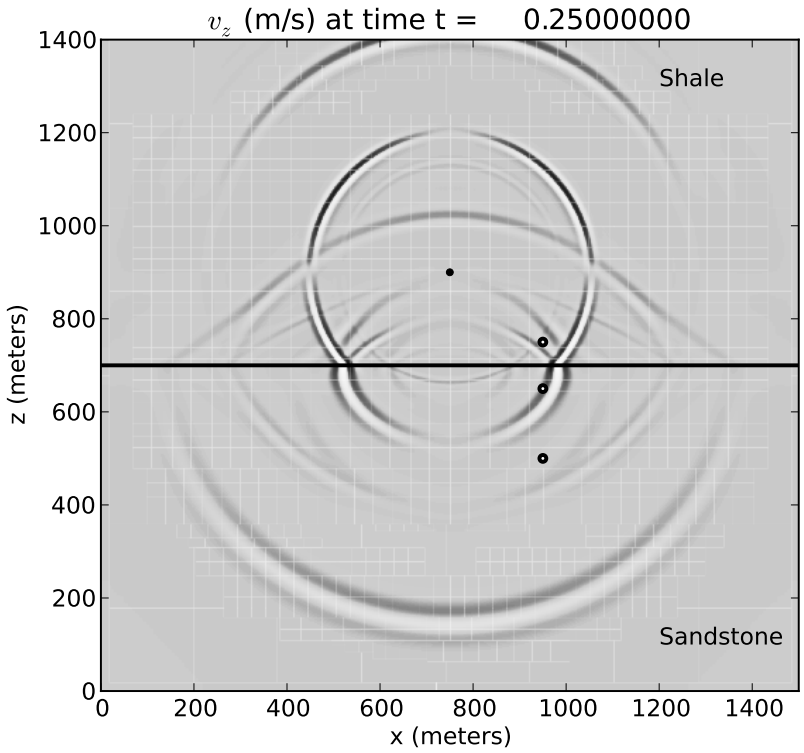

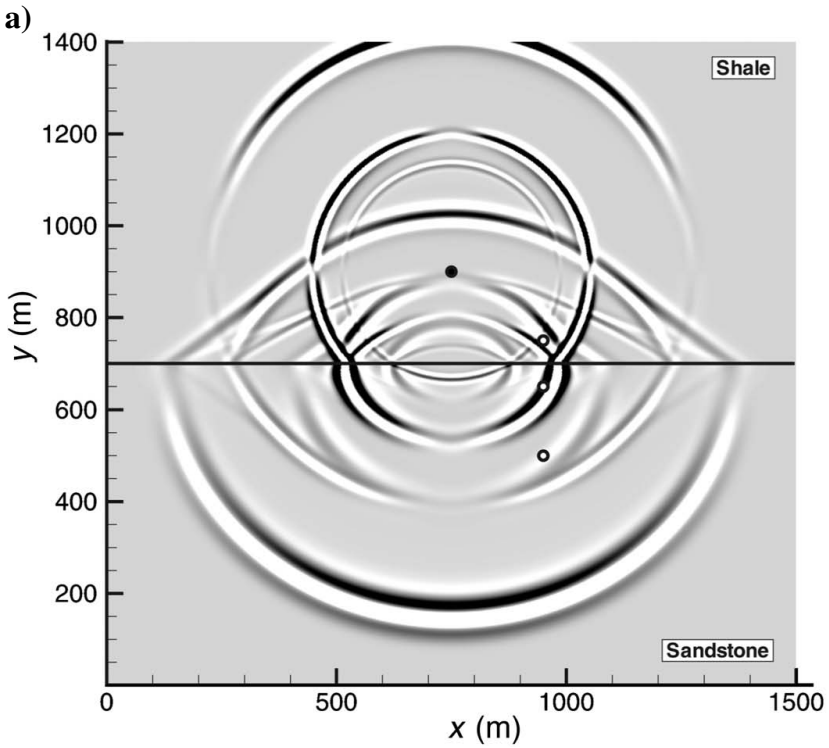

z component of matrix velocity field.
Left: CLAWPACK, right: de la Puente.
Rectangular outlines indicate boundaries of AMR grids.
Note: Different value-to-shade maps on each plot.

Poroelastic code validation: two-material test case

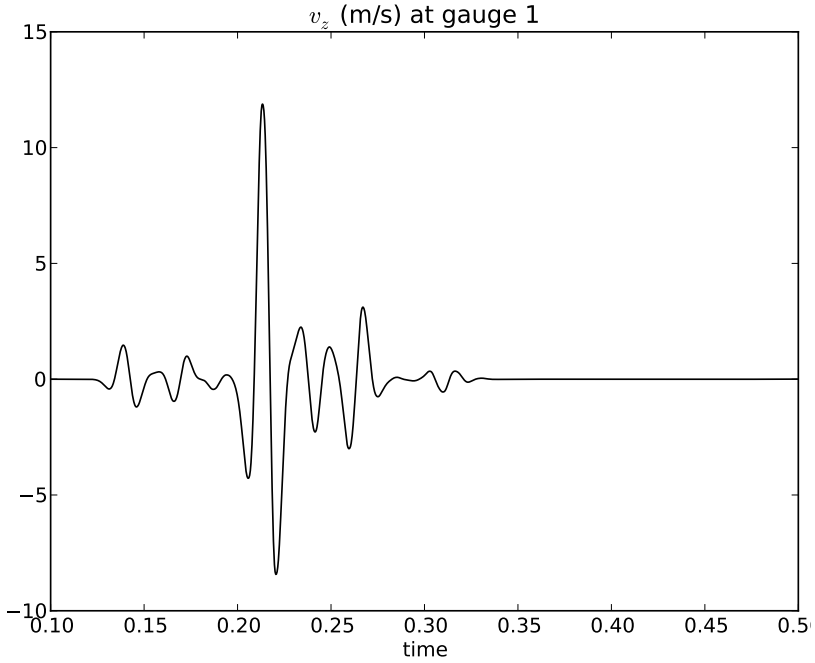

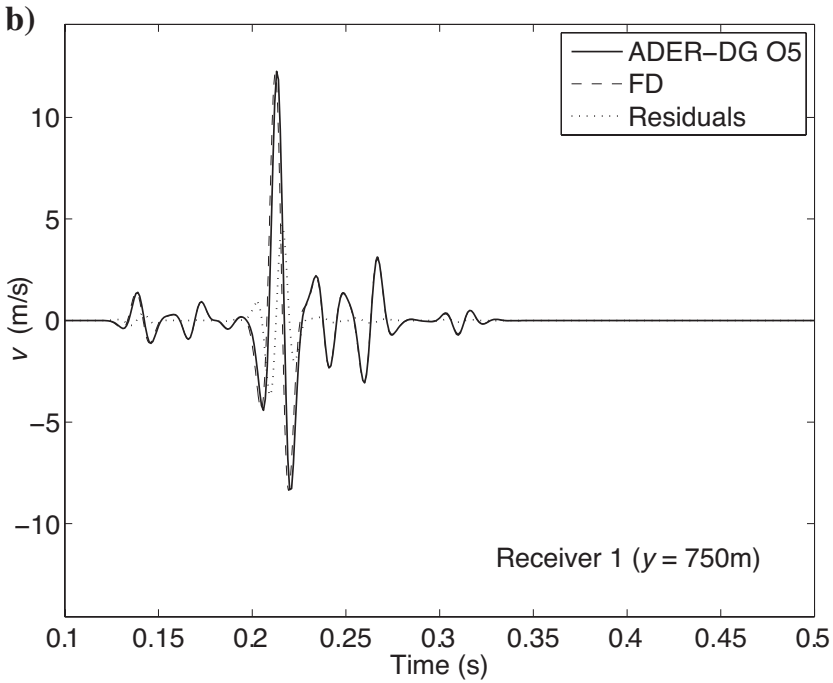

Time-history of matrix z velocity at topmost gauge.
Left: CLAWPACK, right: de la Puente.

Inclusions of different materials

- Can also use mapped grids to model more interesting geometry
- Have some quick results with a circular inclusion of a different poroelastic material (shale in sandstone)
- More complex shapes can be modeled – only requirement is a mapping function
- Also have fluid-poroelastic interface modeling – will be able to combine with mapped grids to model:
  - Fluid-filled lacunae or canals
  - Bone surrounded by fluid
  - Poroelastic seabed (if there's interest)
- Also plan to add poroelastic-nonporous solid interface modeling

Sample results for poroelastic inclusion

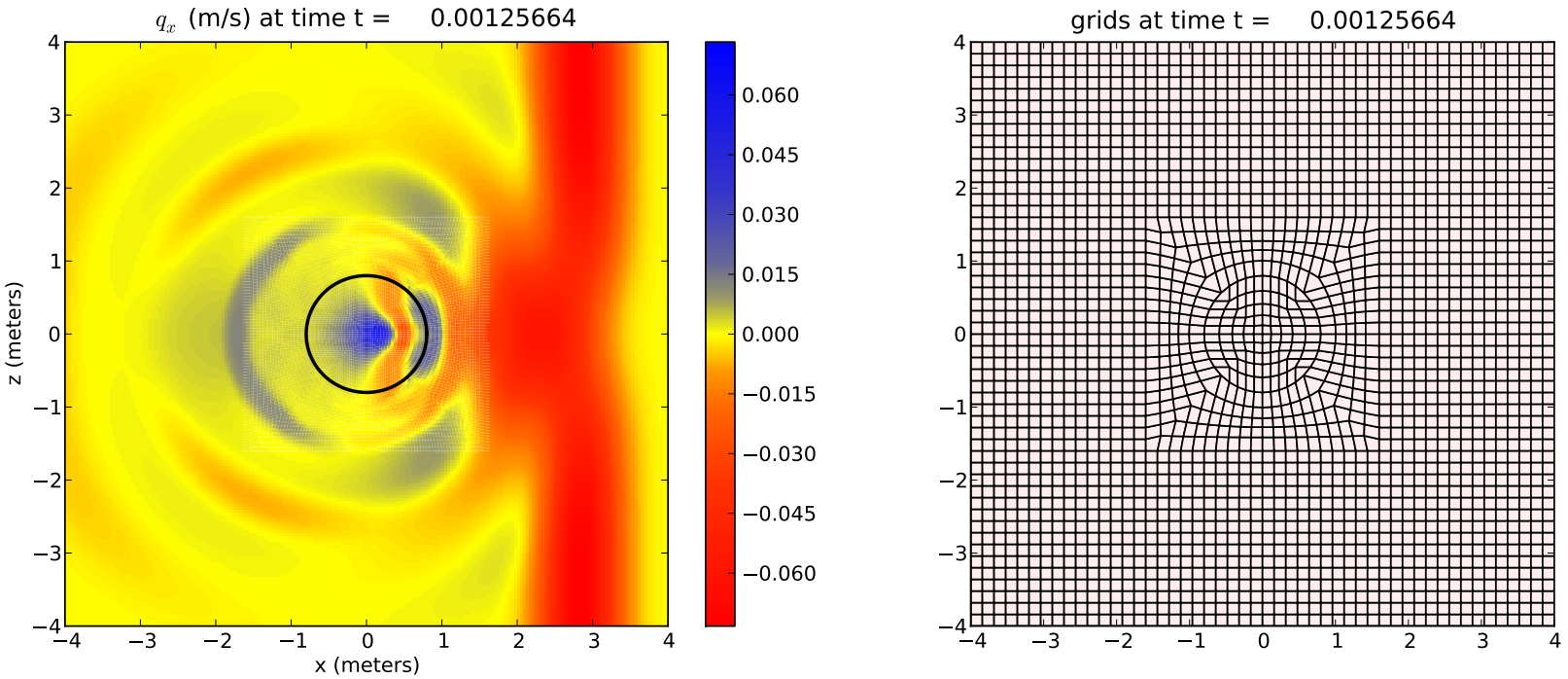

Results for isotropic shale inclusion in isotropic sandstone, struck by fast P-wave with Gaussian profile. Left: x direction fluid velocity (200×200 grid); right: 50×50 grid illustrating mapping Logically rectangular circle map from Calhoun, Helzel, and LeVeque (2007)

Convergence studies

- Conducted convergence studies against analytic solutions
- Solutions used: plane waves of the form

$$Q(x, z, t) = V \exp(i(k_x x + k_z z - \omega t))$$

  with some real ω specified.
- Important to test with waves propagating in variety of directions θ_{wave}
- Also need to test variety of material principal directions θ_{mat}
- For each $(\theta_{\text{wave}}, \theta_{\text{mat}})$ pair, need to sweep over grid size to check convergence

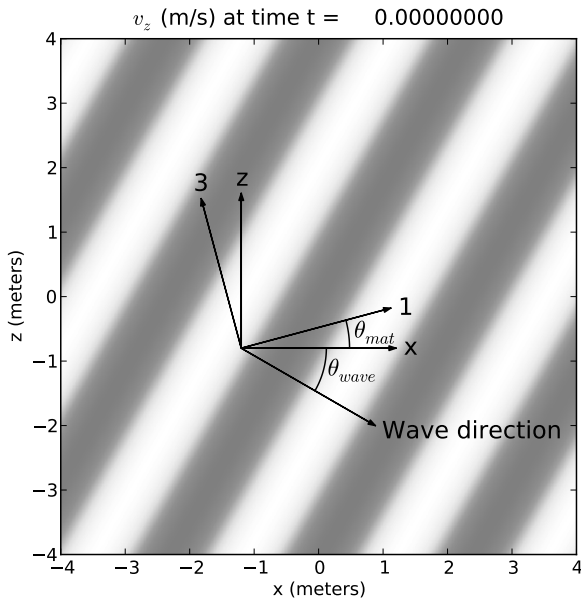

Snapshot of plane wave solution

showing θ_{wave}, principal axes, and θ_{mat}

Convergence results: inviscid

- First convergence study: ignore viscous dissipation, validate hyperbolic solver by itself
- Results are generally good
- Slow P wave was underresolved on coarse grids – worse apparent performance
- Error measured using energy max-norm, relative to amplitude in energy norm of true solution

	Convergence rate		Error on finest grid	
Wave family	Best	Worst	Best	Worst
Fast P	2.02	1.96	5.61×10^{-5}	1.76×10^{-4}
S	2.00	1.96	2.80×10^{-4}	7.98×10^{-4}
Slow P	1.93	1.67	8.81×10^{-3}	3.16×10^{-2}

Convergence results: viscous frequency sweep

- Frequency wasn't important for inviscid case because there's only one time scale (the wave period itself)
- This won't be true when viscosity is included
  - Viscous dissipation has its own time scale, independent of frequency
  - Unknown how operator splitting will perform
- Worth doing a sweep over frequency to see effect of operator splitting
- Kept domain size at constant multiple of wavelength (or dissipation scale for slow P wave)
  - Keeps error from hyperbolic solver roughly constant
  - Isolates effect of operator splitting

Convergence results: viscous frequency sweep

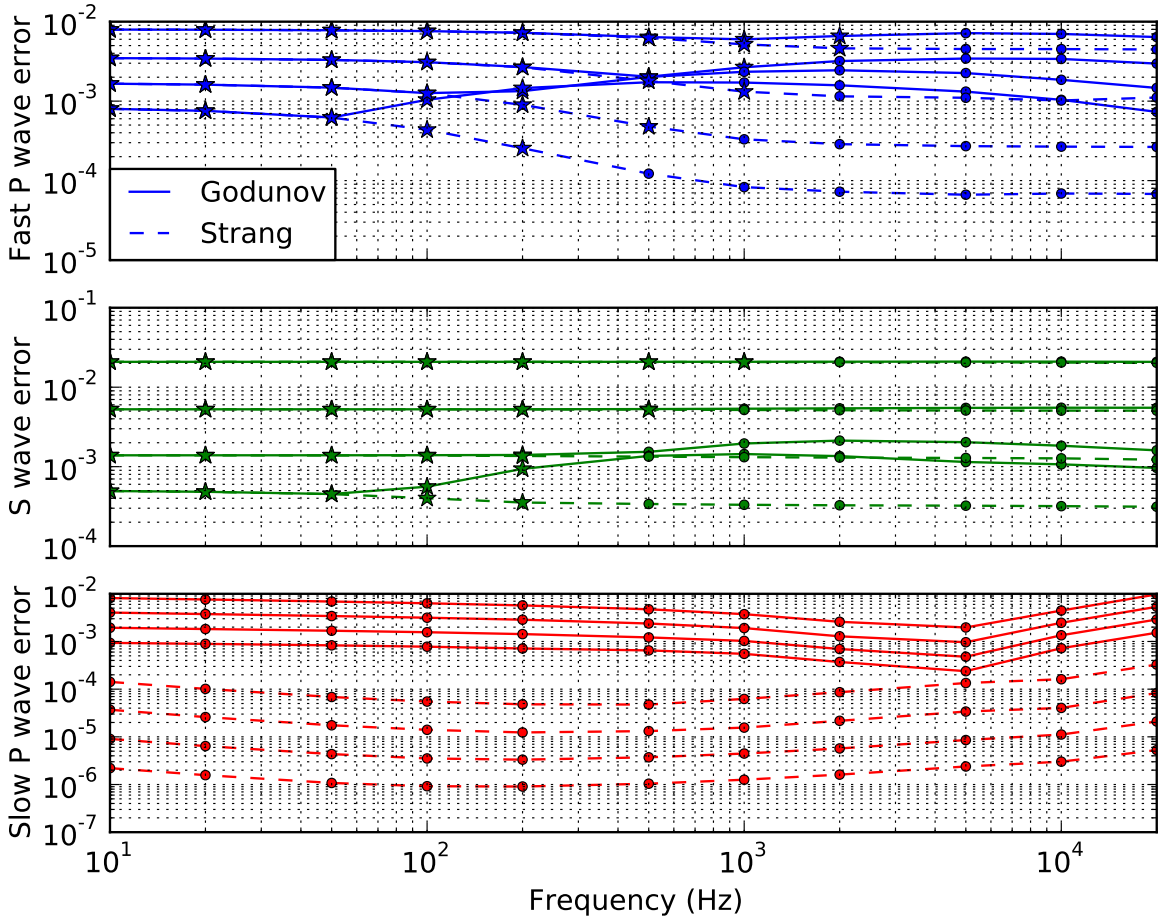

Error vs. frequency for 100×100 through 800×800 grids with Godunov or Strang splitting. Circles: time step less than characteristic dissipation time; stars: time step greater than dissipation time.

Convergence results: viscous high-frequency

- Ran more detailed convergence studies in low-frequency and high-frequency regimes of plot
- High frequency chosen: 10 kHz
- Used Strang splitting for all cases
- Ran slow P waves on different grid from others because of extremely rapid damping
- Results are good, though not as good as inviscid for the fast P and S waves

	Convergence rate		Error on finest grid	
Wave family	Best	Worst	Best	Worst
Fast P	2.05	2.00	6.44×10^{-5}	1.81×10^{-4}
S	2.03	1.99	2.99×10^{-4}	7.59×10^{-4}
Slow P	2.03	1.96	6.53×10^{-6}	2.25×10^{-3}

Convergence results: viscous low-frequency

- Also examined results at low frequency: 10 Hz
- Again ran slow P waves on different grid because of rapid damping
- Used Strang splitting for all cases
- Results are not so good

	Convergence rate		Error on finest grid	
Wave family	Best	Worst	Best	Worst
Fast P	1.61	1.10	3.90×10^{-4}	1.04×10^{-3}
S	1.83	1.36	9.63×10^{-4}	1.92×10^{-3}
Slow P	2.09	1.84	2.40×10^{-6}	4.59×10^{-4}

Convergence results: discussion

What's going on here?

- Trouble only for timesteps comparable to relaxation time or longer
  - Note: asymptotic error estimates only good as $\Delta t \to 0$ – not inconsistent with bad results for Strang at "large" Δt.
- Literature suggests hyperbolic systems with stiff relaxation terms are hard to model
- Dissipation causes change in structure of Riemann solution at longer times
  - Solution structure approaches that of reduced system, but reduced system waves are "blurred" into erf-shapes
- May improve accuracy by modeling this explicitly

Summary

- Poroelasticity is a rich and complex system, with a wide variety of behaviors
- Have developed poroelasticity solver, validated against known solutions
- Solver capabilities:
  - Multiple materials
  - Fluid-poroelastic interfaces
  - Mapped grids for moderately complex geometries
  - Parallel execution (thanks to CLAWPACK framework)
- Convergence rate is suboptimal in the stiff regime, but magnitude of error is generally not bad
- Convergence and accuracy are good away from stiff regime

Future work

- Deal with convergence problems in stiff regime, possibly via more advanced Riemann solver
- Extend to 3D
- Extend to modeling of fluid/solid/poroelastic systems
- Implement property averaging across material boundaries for geometry too complex for mapped grids
- Look at micro-scale modeling to obtain poroelastic properties

Poroelasticity system matrices

$$\breve{A} = n_x A + n_z B = \begin{bmatrix} 0 & \breve{A}_{sv} \\ \breve{A}_{vs} & 0 \end{bmatrix}, \quad D = \begin{bmatrix} 0 & 0 \\ 0 & D_v \end{bmatrix}$$

$$\breve{A}_{sv} = -\begin{bmatrix} -n_x \alpha_1 M & -n_z \alpha_3 M & -n_x M & -n_z M \\ n_x c_{11}^u & n_z c_{13}^u & n_x \alpha_1 M & n_z \alpha_1 M \\ n_x c_{13}^u & n_z c_{33}^u & n_x \alpha_3 M & n_z \alpha_3 M \\ n_z c_{55}^u & n_x c_{55}^u & 0 & 0 \end{bmatrix}$$

$$\breve{A}_{vs} = -\begin{bmatrix} n_x \frac{\rho_f}{\Delta_1} & n_x \frac{m_1}{\Delta_1} & 0 & n_z \frac{m_1}{\Delta_1} \\ n_z \frac{\rho_f}{\Delta_3} & 0 & n_z \frac{m_3}{\Delta_3} & n_x \frac{m_3}{\Delta_3} \\ -n_x \frac{\rho}{\Delta_1} & -n_x \frac{\rho_f}{\Delta_1} & 0 & -n_z \frac{\rho_f}{\Delta_1} \\ -n_z \frac{\rho}{\Delta_3} & 0 & -n_z \frac{\rho_f}{\Delta_3} & -n_x \frac{\rho_f}{\Delta_3} \end{bmatrix}$$

$$D_v = \begin{bmatrix} 0 & 0 & \frac{\rho_f \eta}{\Delta_1 \kappa_1} & 0 \\ 0 & 0 & 0 & \frac{\rho_f \eta}{\Delta_3 \kappa_3} \\ 0 & 0 & -\frac{\rho \eta}{\Delta_1 \kappa_1} & 0 \\ 0 & 0 & 0 & -\frac{\rho \eta}{\Delta_3 \kappa_3} \end{bmatrix}$$

Back to main

Poroelasticity energy matrix

$$E = \begin{bmatrix} E_s & 0 \\ 0 & E_v \end{bmatrix}$$

$$E_s = \begin{bmatrix} \frac{1}{M} + \frac{\alpha_1^2 c_{33}^{(m)} + \alpha_3^2 c_{11}^{(m)} - 2\alpha_1\alpha_3 c_{13}^{(m)}}{c_{11}^{(m)} c_{33}^{(m)} - \left(c_{13}^{(m)}\right)^2} & \frac{\alpha_1 c_{33}^{(m)} - \alpha_3 c_{13}^{(m)}}{c_{11}^{(m)} c_{33}^{(m)} - \left(c_{13}^{(m)}\right)^2} & \frac{\alpha_3 c_{11}^{(m)} - \alpha_1 c_{13}^{(m)}}{c_{11}^{(m)} c_{33}^{(m)} - \left(c_{13}^{(m)}\right)^2} & 0 \\ \frac{\alpha_1 c_{33}^{(m)} - \alpha_3 c_{13}^{(m)}}{c_{11}^{(m)} c_{33}^{(m)} - \left(c_{13}^{(m)}\right)^2} & \frac{c_{33}^{(m)}}{c_{11}^{(m)} c_{33}^{(m)} - \left(c_{13}^{(m)}\right)^2} & -\frac{c_{13}^{(m)}}{c_{11}^{(m)} c_{33}^{(m)} - \left(c_{13}^{(m)}\right)^2} & 0 \\ \frac{\alpha_3 c_{11}^{(m)} - \alpha_1 c_{13}^{(m)}}{c_{11}^{(m)} c_{33}^{(m)} - \left(c_{13}^{(m)}\right)^2} & -\frac{c_{13}^{(m)}}{c_{11}^{(m)} c_{33}^{(m)} - \left(c_{13}^{(m)}\right)^2} & \frac{c_{11}^{(m)}}{c_{11}^{(m)} c_{33}^{(m)} - \left(c_{13}^{(m)}\right)^2} & 0 \\ 0 & 0 & 0 & \frac{1}{c_{55}^{(m)}} \end{bmatrix}$$

$$E_v = \begin{bmatrix} \rho & 0 & \rho_f & 0 \\ 0 & \rho & 0 & \rho_f \\ \rho_f & 0 & m_1 & 0 \\ 0 & \rho_f & 0 & m_3 \end{bmatrix}$$

▸ Back to main